Journal of Alloys and Compounds 509 (2011) 7717–7722

Contents lists available at ScienceDirect

Journal of Alloys and Compounds

journal homepage: www.elsevier.com/locate/jallcom

Microstructure and mechanical properties of Mg–Gd–Dy–Zn alloy with long period stacking ordered structure or stacking faults

Jinghuai Zhang[a], Zhe Leng[a], Shujuan Liu[b], Jiqing Li[a], Milin Zhang[a,*], Ruizhi Wu[a]

[a] Key Laboratory of Superlight Materials & Surface Technology, Ministry of Education, Harbin Engineering University, Harbin 150001, China
[b] Department of Materials Physics and Chemistry, Harbin Institute of Technology, Harbin 150001, China

ARTICLE INFO

Article history:
Received 14 January 2011
Received in revised form 12 April 2011
Accepted 15 April 2011
Available online 23 April 2011

Keywords:
Magnesium alloy
Long period stacking ordered structure (LPSO)
Stacking faults (SF)

ABSTRACT

The Mg–6.5Gd–2.5Dy–1.8Zn (wt.%) alloy with high strength and ductility was prepared by conventional casting method. At room temperature, the as-cast alloy with 14H long period stacking ordered (LPSO) structure exhibits an ultimate tensile strength of 276 MPa and elongation to failure of 10.8%, while they are 392 MPa and 6.1% for the peak-aged alloy with basal plane stacking faults (SF). The results indicate that the kinking of LPSO structure is beneficial for both work hardening and plasticity, and 14H LPSO structure contributes more to the improvement of ductility while SF is more effective in increasing strength.

1. Introduction

Recently, magnesium alloys receive strong research interest for applications to various structural components of automobiles and aircrafts due to the increasing demands for weight reduction, energy saving as well as environment protection [1]. At present, the Mg–RE_1–RE_2-based alloys represented mainly by Mg–Gd–Y–Zr are the best high strength and heat resistant magnesium alloys produced by conventional methods [2–6]. However, due to the high content of RE these precipitation hardening alloys increase their strength at the expense of ductility in most cases [4,7,8]. For example, the ultimate tensile strength of T6 state Mg–10Gd–5Y–0.4Zr (wt.%) alloy at room temperature is above 300 MPa, while its elongation is less than 3% [7]. The poor ductility is unfavorable to their practical application. Therefore, it is important to develop high strength magnesium alloys which also possess sufficient ductility.

Zn is one of the most important elements which can further improve strengthening response of Mg–RE alloys [8–11]. Furthermore, recently the various types of the long period stacking ordered (LPSO) structures, including 6H, 10H, 14H, 18R, 24R types, are observed in the Mg–RE (–RE′)–Zn (RE = Y, Gd, Tb, Dy, Ho, Er, Tm) system [12–32]. It is believed that these LPSO structures can play an important role in the improvement of mechanical properties of alloys [1,7,25–27]. Therefore, the Mg alloys containing LPSO structure are considered to be promising candidates for lightweight structural materials. In addition, the basal plane stacking faults (SF) were also observed in as-cast $Mg_{97}Zn_1Y_2$ (at.%) alloy [27], as-cast Mg–10Gd–3Y–1.2Zn–0.4Zr (wt.%) [33] alloy and $Mg_{97}Zn_1Gd_2$ (at.%) alloy aged at 573 K for 10 h [26], but the effect of SF on the mechanical properties of these Mg alloys were rarely reported. On the other hand, the first principle calculation was carried out to study the SF in LPSO structure recently [33–36]. Based on the SF energy calculation, Datta et al. [33] reported that in an Mg–Zn–Y alloy Y stabilizes the long periodicity, while its mechanical properties are further improved due to Zn doping, and they also corroborated that an increase in stacking periodicity can initiate activation of non-basal slip in the system and thereby improve ductility of the alloy.

Now the Mg–Gd-based alloys are the typical magnesium alloys with heat resistance and high strength. Considering that Dy element has the similar radii and physical/chemical properties to that of Gd, moreover, both of them can form LPSO structure with Zn [25], therefore better mechanical properties may be achieved if a small amount of Zn is added into Mg–Gd–Dy alloy. Bearing in mind all the facts mentioned above, in this work a new Mg–6.5Gd–2.5Dy–1.8Zn (wt.%) alloy fortified by LPSO structure or SF has been developed by conventional casting method, and it exhibits high strength and good ductility.

2. Experimental procedures

The alloy ingot with actual composition of Mg–6.5Gd–2.5Dy–1.8Zn (GDZ732, wt.%) was prepared from commercial purity Mg, Zn, Mg-25 wt.% Gd and Mg-20 wt.% Dy master alloys in an electric resistance furnace with a graphite crucible under an anti-oxidizing flux. The alloying melt was homogenized at about 750 °C for 0.5 h. Then, it was poured into a preheated (~200 °C) steel mould at approximately 720 °C.

* Corresponding author. Tel.: +86 451 82533026; fax: +86 451 82533026.
E-mail address: jinghuaizhang@gmail.com (M. Zhang).

0925-8388/$ – see front matter © 2011 Elsevier B.V. All rights reserved.
doi:10.1016/j.jallcom.2011.04.089

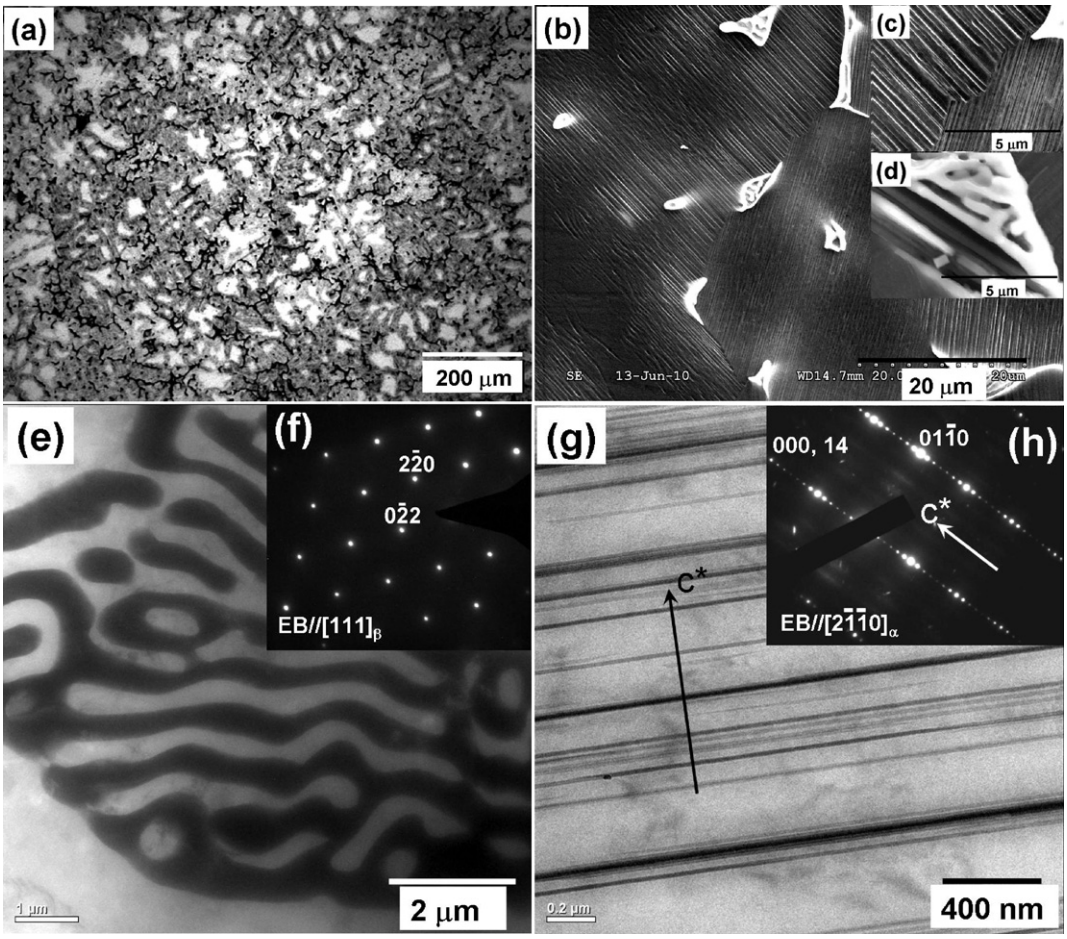

Fig. 1. Microstructure of the as-cast sample: (a) OM image; (b), (c) and (d) SEM image; (e) TEM image of Mg_3Gd-type compound and (f) corresponding SAED pattern; (g) TEM image of 14H LPSO structure and (h) its SAED pattern.

The size of the ingot is 100 mm × 100 mm × 30 mm. Practical chemical composition was determined by inductively coupled plasma atomic emission spectroscopy (ICP-AES). The heat treatment sample was solution treated at 510 °C for 10 h and then quenched into hot water at about 60 °C (T4), and a subsequent aging treatment was preformed at 215 °C and 315 °C, respectively.

The microstructure of as-cast and heat-treated alloys was investigated by optical microscope (OM), scanning electron microscope (SEM) equipped with an X-ray energy-dispersive spectrometer (EDS), transmission electron microscopy (TEM). The hardness measurement was carried out by Vickers hardness (Hv) tester, and the test load and application time were 50 g and 15 s, respectively. The specimens for tensile test are dumbbell test pieces with the gauge size of 35 mm × 5 mm × 3 mm. The tensile tests were carried out using a standard tensile testing machine at room and elevated temperatures under a strain rate of $8.33 \times 10^{-4}\ s^{-1}$. The value of the tensile tests in the study was the average of at least four measurements.

3. Results and discussion

3.1. Microstructure

Fig. 1(a) shows the optical micrograph of as-cast GDZ732 alloy. At low magnification, it reveals that the as-cast alloy is mainly composed of equiaxed dendrites and partially interdendritic eutectics, which is the typical microstructure of casting-processed Mg alloys with relatively low cooling rate. However, compared with the microstructure of Mg–Gd–Dy alloy without Zn [37], the dramatic difference is that besides the dendrites, obviously additional gray region occupies most α-Mg matrix.

Fig. 1(b)–(d) shows the SEM images of the as-cast GDZ732 alloy. Four phases: α-Mg, island-like eutectic compound as β-phase, fine lamellae (see Fig. 1(b), corresponding to gray region in Fig. 1(a)) and very few amounts of cuboid-shaped phase (see Fig. 1(d)) can be found. The fine lamellae uniformly distribute from grain boundaries to the interior of α-Mg grains; these lamellae are orientated in one direction within a grain (Fig. 1(b) and (c)), which suggests that the lamellar phase has specific orientation relationship with the α-Mg matrix. In addition, it is noted that some lamellae run through the whole grain but some not, and the lamellae are scarce at the center of some large size grains, which suggests the variation of chemical composition in these grains. Chemical analyses by the EDS in SEM mode reveal that the averaged compositions of the eutectic compound are Mg–10.31 ± 1.0Gd–2.85 ± 1.0Dy–10.69 ± 1.0Zn (at.%), therefore, the eutectic compound can be described as Mg_3(Gd, Dy, Zn). Fig. 1(e) and (f) shows the TEM micrograph of eutectic compound and the corresponding selected area electron diffraction (SAED) pattern with the electron beam parallel to the [1 1 1] zone, respectively. The SAED pattern reveals that it is a Mg_3Gd-type compound with a face centered cubic (fcc) structure. The lamellar phase and cuboid-shape phase are too small to be determined by EDS in SEM mode. Ding et al. [28] reported that the similar small cuboid-shape particle is $Gd_{17}Mg_3$ in Mg–Gd–Zn alloy. In Fig. 1(g) and (h) the TEM micrograph of lamellae and the corresponding SAED pattern is shown with the zone axis of $[2\,\bar{1}\,\bar{1}\,0]_\alpha$, respectively. The SAED pattern shows 12 extra spots divide the correlation length of $(0\,0\,0\,2)_\alpha$ (corresponding to $(0\,0\,0,\,14)_{LPSO}$), which identifies the lamellae as 14H LPSO structure.

Fig. 2(a)–(c) shows the comparative observation of the as-cast, T4 treated and peak-aged (T6) samples at the same magnification, respectively. After 10 h of solution treatment at 510 °C, the

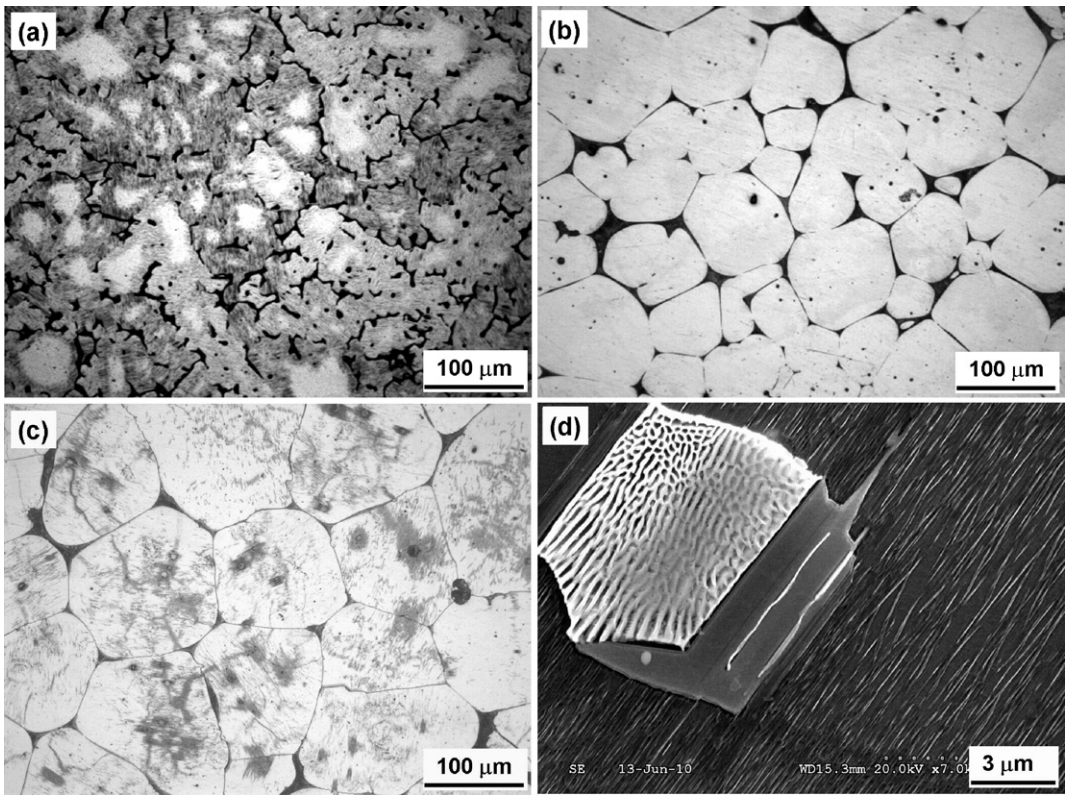

Fig. 2. Optical images of the (a) as-cast, (b) T4 treated and (c) peak-aged (T6) samples; (d) magnified SEM image of the peak-aged sample.

dendrites and the lamellar 14H LPSO structure disappear and the eutectics dissolve partly and are redistributed along the grain boundaries. The dramatic change of microstructure can be observed between the T4 state and the T6 state. As shown in Fig. 2(c), after aging at 215 °C for 109 h (i.e. peak-aged state), a large number of dispersed precipitates appear in the matrix and the eutectics along the grain boundaries dissolve further. At magnified SEM observation (Fig. 2(d)), it reveals that plenty of fine needle-like precipitates are distributed uniformly in the grains and orientated in one direction within a grain; in addition, notice that some polygonal or quasi-circular Mg_3(Gd, Dy, Zn) eutectic compounds appear at the grain inner and the number density of needle-like precipitates is higher around them, indicating that their formation is closely related.

Fig. 3(a) and (b) shows the TEM images of the needle-like precipitates. Note that besides the relatively long needle-like precipitates, even more fine and dispersed needle-like precipitates with length of 30–50 nm are observed in the matrix. Fig. 3(c) presents the dislocation morphology between the needle-like precipitate and the matrix. The high-resolution TEM (HRTEM) image in Fig. 3(d) and SAED patterns with streaks between the diffraction spots along *c*-axis in Fig. 3(e) and (f) confirm that the needle-like precipitates mentioned above are basal plane stacking faults (SF).

In this study, the outstanding microstructure of as-cast Mg–Gd–Dy–Zn alloy is the lamellar 14H LPSO structure within α-Mg matrix formed originally during solidification as well as Mg_3Gd-type eutectic compound as the secondary phase. According to the research by Ding et al. [28], the formation mechanism of LPSO is considered to be a nucleation-growing one. Note that in the as-cast state the lamellar 14H LPSO structure is observed from the dendrite boundary to the interior of dendrite as more Gd, Dy and Zn atoms enrich in dendrite boundaries. However, it is noticed that in the peak-aged state the SF tends to be dispersed in the interior of grains. We speculate that the SF is formed in two ways, that is, precipitation from supersaturated α-Mg matrix and transformation from Mg_3(Gd, Dy, Zn) eutectic compound phase (see Fig. 2(d)).

It is well known that the Mg–Gd (-RE)-based alloys exhibit a four-stage precipitation sequence during aging at about 200–250 °C: α (ssss) → β″ ($D0_{19}$ Mg_3RE) → β′ (bco $Mg_{15}RE_3$) → β_1 (fcc) → β (fcc Mg_5RE), and the main strengthening phase of the peak-aged alloy (T6 state) is β′ metastable phase [8,38]. Recently, in the Mg–Gd–Zn alloys Yamasaki et al. [26] proposed a three-step precipitation sequence during aging at 200 °C: α (ssss) → β′ (orthor, Mg_7Gd) → β_1 (fcc, Mg_5Gd) → β (fcc Mg_5Gd). However, in Mg–Gd–Dy–Zn alloy, the lamellar 14H LPSO structure disappears during solution heat treatment at 510 °C for 10 h, while SF are observed during the following peak-aging at 215 °C for 109 h. A simple precipitation sequence is proposed: α (ssss) → SF. We consider that the SF is the preceding stage of formation of LPSO structure. HAADF-STEM observations by Yamasaki et al. [26] revealed that Zn and Gd atoms concentrate in two atomic layers sandwiching a SF in the Mg–Gd–Zn alloy. Suzuki et al. [39] suggested that the SF energy in the Mg matrix decreases with the simultaneous existence of Zn and Y. Based on the previous researches, as the formation of SF from supersaturated α-Mg matrix in Mg–Gd–Dy–Zn alloy, it appears to occur due to a diffusion-controlled process in aging treatment where relatively high temperature and long time allow the full diffusion of Gd, Dy and Zn atoms and subsequently lead to minimum total energy in the systems, consequently, the SF concentrating Gd, Dy and Zn atoms is formed. The detailed experimental work of whole sequence is now in progress.Mechanical properties

Fig. 4 shows the age hardening curves of the T4 treated alloy. The obvious age-hardening response is exhibited at the aging temperatures in GDZ732 alloy. The hardness of T4 treated alloy is 68 Hv, while the peak hardness of 142 Hv is obtained when aged at 215 °C for 109 h (T6 state), which is 2 times higher than that of T4 treated alloy.

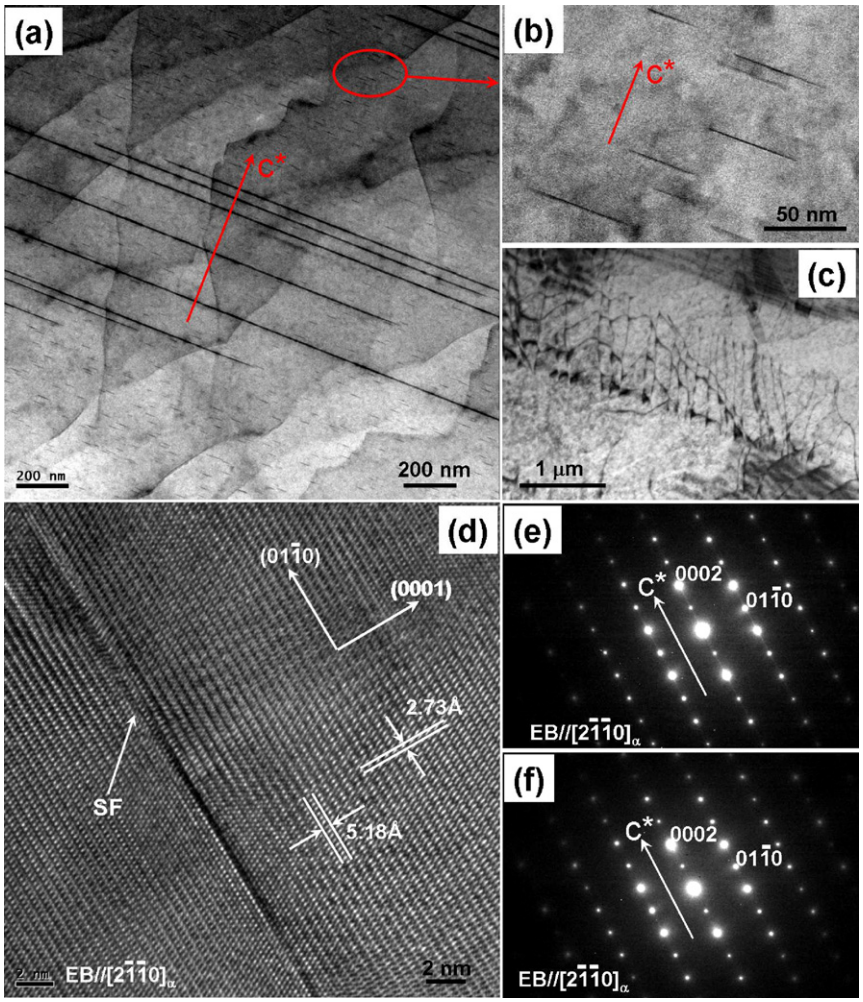

Fig. 3. (a), (b) and (c) TEM images of SF in peak-aged sample; (d) HRTEM image of SF in peak-aged sample; (e) SAED pattern from the long needle-like SF; (f) SAED pattern from the fine needle-like SF.

Fig. 5 shows the engineering tensile stress-strain curves of GDZ732 alloy at room temperature (RT) and 250 °C. The tensile properties including ultimate tensile strength (UTS), tensile yield strength (TYS), elongation to failure (ε) and work hardening exponent (n) of GDZ732 alloys are shown in Table 1. As Ref. [37], the tensile properties of Mg–8Gd–1Dy–0.4Zr (wt.%) alloy are also listed. As shown, the Mg–Gd–Dy–Zn alloy in the present work exhibits higher strength and elongation compared with Mg–Gd–Dy–Zr alloy without Zn. In as-cast state, the GDZ732 alloy exhibits relatively high strength and good ductility, and the values of UTS and ε are 276 MPa and 10.8% at RT, respectively. T6 heat treatment could enhance the tensile strength of GDZ732 alloy. Especially the UTS (392 MPa) and TYS (295 MPa) of the peak-aged alloy are dramatically increased by more than 100 MPa at RT. Although the elongation decreases both at room and elevated temperatures after T6 heat treatment, it also can reach 6% at RT and 12% at 250 °C. Moreover, by examining the TYS, UTS and n, it is clear that the alloys exhibit considerable work hardening.

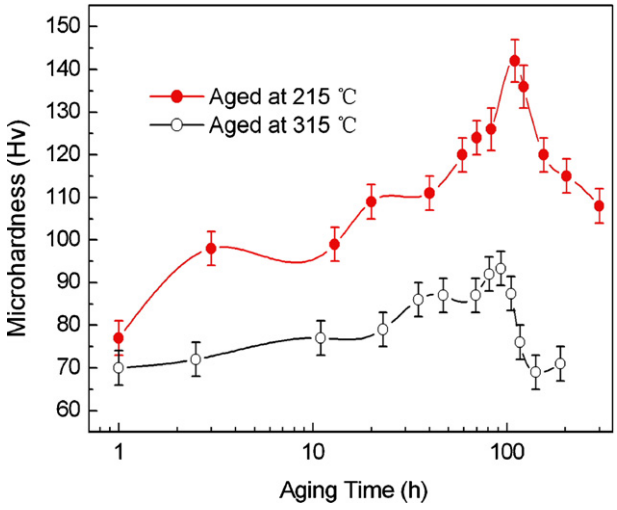

Fig. 4. Age-hardening response of solution treated samples.

It has been reported that the hardness value for different types of LPSO structures (137 [19], 87 [21] and 161 [40]) is higher than that of Mg matrix. Moreover, Mastsuda et al. [41] have reported that the critical resolved shear stress of the basal plane increases due to the formation of the LPSO structure. Thus, the LPSO structure can provide important strengthening sources in the alloy. In this work, we show SEM observations (Fig. 6) of the longitudinal section near the fracture of the as-cast GDZ732 alloy, which could partly explains the high ductility and work hardening of alloys containing LPSO structure. It can be seen that kink bands are formed in the LPSO structure. In addition, there were no cracks large enough to be observed within or around the kinked LPSO structure. These

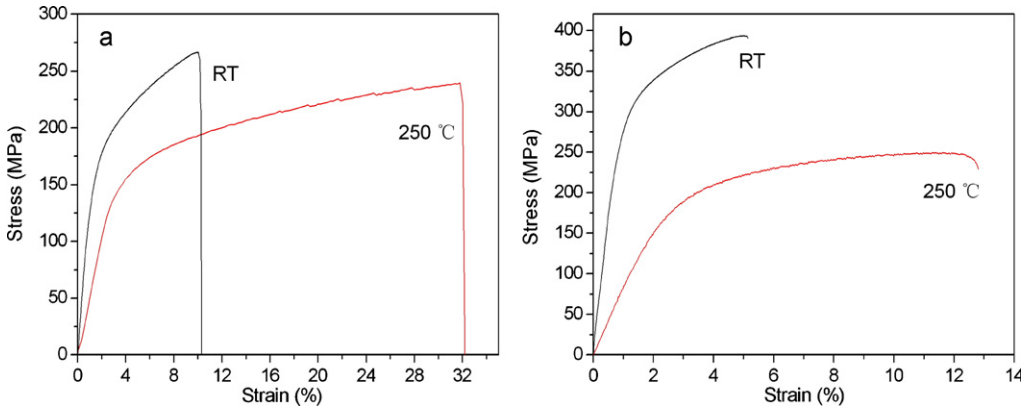

Fig. 5. The representative engineering stress-strain curves of GDZ732 alloy: (a) as-cast state; (b) peak-aged state.

Table 1
Mechanical properties of Mg–6.5Gd–2.5Dy–1.8Zn and Mg–8Gd–1Dy–0.4Zr alloys.

Alloy (wt.%)	State	UTS (MPa)		TYS (MPa)		ε (%)		n	
		RT	250 °CC	RT	250 °C	RT	250 °C	RT	250 °C
GDZ732 (this work)	As-cast	276	240	145	130	10.8	33.8	0.32	0.30
	Peak-aged	392	247	295	152	6.1	12.0	0.22	0.27
Mg8Gd1Dy0.4Zr	As-cast	210	187	131	116	5.7	7.9	/	/
[37]	Peak-aged	355	230	261	174	3.8	7.4	/	/

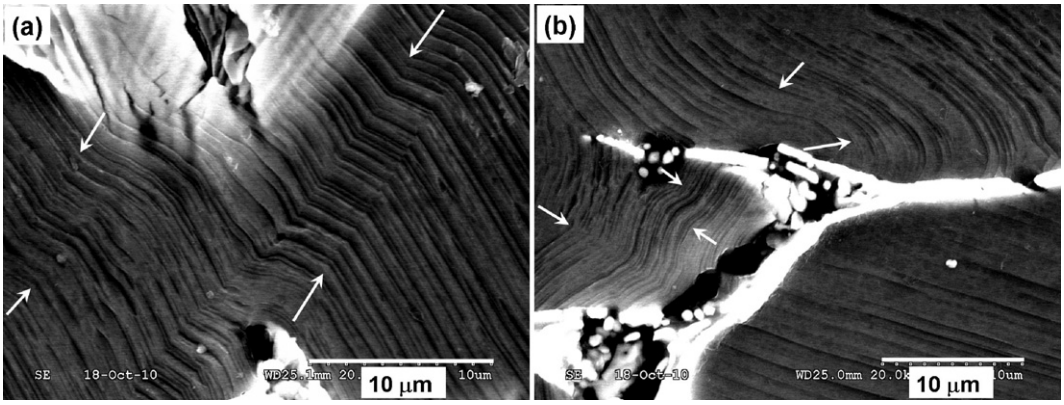

Fig. 6. SEM images of the longitudinal section of fractured tensile specimens at (a) RT and (b) 250 °C.

suggest that the LPSO structure causes no drastic change in nature of metallic bonding of atoms [19]. Chino et al. [19] reported that no microcracks were observed around the indentation at the matrix region with the LPSO structure for the Vickers hardness tests, and based on the above observation, they pointed out that one of the features for LPSO structure is preservation in high ductility, which is in general accordance with our experimental results (Figs. 5 and 6). Furthermore, Shao et al. [27] investigated the deformation behavior and corresponding microstructure evolution of a $Mg_{97}Zn_1Y_2$ (at.%) alloy with LPSO structure subjected to hot compression, and reported that kinking of the LPSO structure itself as well as its transplantation into the Mg matrix could afford considerable amount of plastic deformation to the material, which is important for the ductility of the alloy. They also pointed out that the Vickers microhardness of kinked LPSO structure is much higher than that of LPSO structure in as cast alloy, as a result of work hardening. Therefore, we have reason to believe that kinking of the LPSO structure could contribute to the work hardening whether during compression or tension.

Tensile testing and microstructure observations show a significant difference between the as-cast and peak-aged GDZ732 alloys. The tensile ductility of as-cast alloy with 14H LPSO structure is higher than that of the peak-aged alloy with SF, while the tensile strength of the latter is much higher than that of the former. This result suggests that compared LPSO structure with SF the former benefits more to improving the ductility while the latter is more effective in increasing strength.

4. Conclusions

The Mg–6.5Gd–2.5Dy–1.8Zn alloy with high strength and ductility was prepared successfully by conventional metal mould casting method. The lamellar 14H LPSO structure is observed from dendrite boundary to inner in as-cast state, and SF forms and disperses in the interior of grain in peak-aged state. The ultimate tensile strength of 276 MPa and elongation to failure of 10.8% are obtained from as-cast state at room temperature, and the corresponding values are 392 MPa and 6.1% for the peak-aged state. The results suggest that deformation kinking of LPSO structure is important for both the work hardening and the plasticity, and 14H LPSO structure is more beneficial to the improvement of ductility while SF contributes more to the strength.

Acknowledgements

This work was supported by the Key Project of Science and Technology of Harbin City (2010AA4BE031), the Fundamental Research funds for the Central Universities (HEUCF101008), China Postdoctoral Science Foundation (20100471015, 20100471046), the Heilongjiang Postdoctorial Fund (LBH-Z09217) and the Natural Science Foundation for Youths of Heilongjiang Province of China (QC2010032).

References

[1] K. Hagihara, A. Kinoshita, Y. Sugino, M. Yamasaki, Y. Kawamura, H.Y. Yasuda, Y. Umakoshi, Acta Mater. 58 (2010) 6282–6293.
[2] B.L. Xiao, Q. Yang, J. Yang, W.G. Wang, G.M. Xie, Z.Y. Ma, J. Alloys Compd. 509 (2011) 2879–2884.
[3] X. Zhang, C. Tang, Y. Deng, L. Yang, W. Liu, J. Alloys Compd. (2011), doi:10.1016/j.jallcom.2011.03.059.
[4] V. Janik, D.D. Yin, Q.D. Wang, S.M. He, C.J. Chen, Z. Chen, C.J. Boehlert, Mater. Sci. Eng. A 528 (2011) 3105–3112.
[5] S.M. He, X.Q. Zeng, L.M. Peng, X. Gao, J.F. Nie, W.J. Ding, J. Alloys Compd. 427 (2007) 316–323.
[6] M. Sun, G. Wu, J. Dai, W. Wang, W. Ding, J. Alloys Compd. 494 (2010) 426–433.
[7] J. Wang, J. Meng, D. Zhang, D. Tang, Mater. Sci. Eng. A 456 (2007) 78–84.
[8] T. Honma, T. Ohkubo, S. Kamado, K. Hono, Acta Mater. 55 (2007) 4137–4150.
[9] A.A. Luo, R.K. Mishra, A.K. Sachdev, Scripta Mater. 64 (2011) 410–413.
[10] J.F. Nie, X. Gao, S.M. Zhu, Scripta Mater. 53 (2005) 1049–1053.
[11] D. Wu, R.S. Chen, E.H. Han, J. Alloys Compd. 509 (2011) 2856–2863.
[12] G. Bi, D. Fang, L. Zhao, J. Lian, Q. Jiang, Z. Jiang, Mater. Sci. Eng. A 528 (2011) 3609–3614.
[13] S. Zhang, G.Y. Yuan, C. Lu, W.J. Ding, J. Alloys Compd. 509 (2011) 3515–3521.
[14] K. Liu, J. Meng, J. Alloys Compd. 509 (2011) 3299–3305.
[15] J. Yi, B. Tang, P. Chen, D. Li, L. Peng, W. Ding, J. Alloys Compd. 509 (2011) 669–674.
[16] E. Abe, Y. Kawamura, K. Hayashi, A. Inoue, Acta Mater. 50 (2002) 3845–3857.
[17] K. Liu, J. Zhang, G. Su, D. Tang, L.L. Rokhlin, F.M. Elkin, J. Meng, J. Alloys Compd. 481 (2009) 811–818.
[18] M. Nishida, Y. Kawamura, T. Yamamuro, Mater. Sci. Eng. A 375–377 (2004) 1217–1223.
[19] Y. Chino, M. Mbuchi, S. Hagiwara, H. Iwasaki, A. Yamamoto, H. Tsubakino, Scripta Mater. 51 (2004) 711–714.
[20] Y.J. Wu, X.Q. Zeng, D.L. Lin, L.M. Peng, W.J. Ding, J. Alloys Compd. 477 (2009) 193–197.
[21] T. Itoi, T. Seimiya, Y. Kawamura, M. Hirohashi, Scripta Mater. 51 (2004) 107–111.
[22] M. Yamasaki, T. Anan, S. Yoshimoto, Y. Kawamura, Scripta Mater. 53 (2005) 799–803.
[23] M. Matsuda, S. Ii, Y. Kawamura, Y. Ikuhara, M. Nishida, Mater. Sci. Eng. A 393 (2005) 269–274.
[24] Y. Kawamura, T. Kasahara, S. Izumi, M. Yamasaki, Scripta Mater. 55 (2006) 453–456.
[25] Y. Kawamura, M. Yamasaki, Mater. Trans. 48 (2007) 2986–2992.
[26] M. Yamasaki, M. Sasaki, M. Nishijima, K. Hiraga, Y. Kawamura, Acta Mater. 55 (2007) 6798–6805.
[27] X.H. Shao, Z.Q. Yang, X.L. Ma, Acta Mater. 58 (2010) 4760–4771.
[28] W.J. Ding, Y.J. Wu, L.M. Peng, X.Q. Zeng, G.Y. Yuan, J. Mater. Res. 24 (2009) 1842–1854.
[29] Y.M. Zhu, A.J. Morto, J.F. Nie, Acta Mater. 58 (2010) 2936–2947.
[30] P. Chen, D. Li, J. Yi, B. Tang, L. Peng, W. Ding, J. Alloys Compd. 485 (2009) 672–676.
[31] Y. Gao, Q. Wang, J. Gu, Y. Zhao, Y. Tong, D. Yin, J. Alloys Compd. 477 (2009) 374–378.
[32] D.J. Li, X.Q. Zeng, J. Dong, C.Q. Zhai, W.J. Ding, J. Alloys Compd. 468 (2009) 164–169.
[33] A. Datta, U.V. Waghmare, U. Ramamurty, Acta Mater. 56 (2008) 2531–2539.
[34] A. Datta, U. Ramamurty, S. Ranganathan, U.V. Waghmare, Comp. Mater. Sci. 37 (2006) 69–73.
[35] T.W. Fan, B.Y. Tang, L.M. Peng, W.J. Ding, Scripta Mater. 64 (2011) 942–945.
[36] J.X. Yi, B.Y. Tang, P. Chen, D.L. Li, L.M. Peng, W.J. Ding, J. Alloys Compd. 509 (2011) 669–674.
[37] Q. Peng, H. Dong, L. Wang, Y. Wu, L. Wang, Mater. Sci. Eng. A 477 (2008) 193–197.
[38] X. Gao, S.M. He, X.Q. Zeng, L.M. Peng, W.J. Ding, J.F. Nie, Mater. Sci. Eng. A 431 (2006) 322–327.
[39] M. Suzuki, T. Kimura, J. Koike, K. Maruyama, Scripta Mater. 48 (2003) 997–1002.
[40] D.D. Yin, Q.D. Wang, Y. Gao, C.J. Chen, J. Zheng, J. Alloys Compd. 509 (2011) 1696–1704.
[41] M. Matsuda, S. Ando, M. Nishida, Mater. Trans. 46 (2005) 361–364.